



Optical sideband spectroscopy of a single ion in a Penning trap

S. Mavadia, G. Stutter, J. F. Goodwin, D. R. Crick, R. C. Thompson, and D. M. Segal*

QOLS Group, Physics Department, Imperial College London, London SW7 2AZ, United Kingdom

(Received 3 December 2013; published 6 March 2014)

We perform resolved optical sideband spectroscopy on a single $^{40}\text{Ca}^+$ ion in a Penning trap. We probe the electric quadrupole allowed $S_{1/2} \leftrightarrow D_{3/2}$ transition at 729 nm and observe equally spaced sidebands for the three motional modes. The axial mode, parallel to the trap axis, is a one-dimensional harmonic oscillator, whereas the radial cyclotron and magnetron modes are circular motions perpendicular to the magnetic field. The total energy associated with the magnetron motion is negative, but here we probe only the (positive) kinetic energy. From the equivalent Doppler widths of the sideband spectra corresponding to the three motions we find effective temperatures of 1.1 ± 0.2 mK, 7 ± 3 mK, and 42 ± 8 μK for the axial, modified cyclotron, and magnetron modes, respectively. These should be compared to the cooling limits, estimated using optimal laser parameters, of 0.38 mK, 0.8 mK, and ~ 10 μK . In future work we aim to perform resolved-sideband cooling of the ion on the 729-nm transition.

DOI: [10.1103/PhysRevA.89.032502](https://doi.org/10.1103/PhysRevA.89.032502)

PACS number(s): 32.30.Jc, 03.67.Lx, 37.10.Ty, 42.62.Fi

I. INTRODUCTION

Vibrational sidebands due to the bound motion of ions in external trapping fields were initially observed on the internal electronic spectra of singly charged ions in radio-frequency (rf) traps using both optical [1] and microwave [2] transitions. Since then, motional sidebands have also been observed in the spectra of microresonators [3] and atoms in optical lattices [4] and tweezers [5,6]. The observation of sidebands is a vital step towards implementing optical sideband cooling of a trapped particle to the lowest energy level of the confining harmonic potential [7]. Trapped ions with well-defined spin and motional states in a radio-frequency trap have been used as a resource for complex quantum computing protocols or quantum simulations (e.g., [8]). However, in these cases the ions will experience micromotion if they are not at the rf null. For this reason, only single ions and linear strings of ions have been used in quantum information studies in a linear rf trap. In principle, Penning traps [9], where the confinement is provided by only a homogeneous magnetic field and a dc electric field, offer an alternative that may allow two- or even three-dimensional structures to be cooled to the ground state without any micromotion (i.e., with constant interparticle distances). Furthermore, a trap of this kind offers the potential to manipulate the quantum state of more particles than has currently been shown to be possible in rf traps [10]. Already, spin-motional-state entanglement has been used to measure the temperature of the motional modes transverse to a planar two-dimensional Coulomb crystal consisting of several hundred ions in a Penning trap [11].

II. PENNING TRAP

In this paper we investigate the three harmonic modes of a single ion in a Penning trap. The trap potential, generated by suitable electrodes, has the form $\phi(r, z) = A(2z^2 - r^2)$, where A is proportional to the applied trap voltage. This defines the position of zero potential energy at the center of the trap.

From this equation we find the angular frequency of the axial motion, $\omega_z = \sqrt{4eA/m}$, where e/m is the charge-to-mass ratio of the particle. The negative radial electrostatic potential energy, combined with the force due to the magnetic field B , gives rise to circular motion at the modified cyclotron (ω_+) and magnetron (ω_-) frequencies, $\omega_{\pm} = \Omega/2 \pm \omega_1$, where $\Omega = eB/m$ and $\omega_1 = \sqrt{\Omega^2/4 - \omega_z^2}/2$.

The axial motion is a conventional simple harmonic oscillation with a positive potential energy whose average value is equal to the average kinetic energy. However, the potential energy of both the cyclotron and magnetron motions is negative relative to the center of the trap. When the kinetic energy and potential energy of each motion are added together, the total energy for the cyclotron mode becomes positive while the magnetron mode energy remains negative. The total energy of the particle can then be written as [12,13]

$$E_{\text{tot}} = \frac{m}{2} [\omega_z^2 Z^2 + 2\omega_1(\omega_+ R_+^2 - \omega_- R_-^2)], \quad (1)$$

where Z , R_+ , and R_- are the amplitudes of the axial, modified cyclotron, and magnetron motions, respectively.

The quantum-mechanical energy levels for the axial, modified cyclotron, and magnetron modes can be written as $E_z = (n_z + 1/2)\hbar\omega_z$, $E_+ = (n_+ + 1/2)\hbar\omega_+$, and $E_- = -(n_- + 1/2)\hbar\omega_-$, respectively, where n represents the quantum occupation number. Setting the energies in the quantum and classical descriptions equal to each other and ignoring the zero-point energy, we find that [13]

$$n_z \simeq m\omega_z Z^2 / 2\hbar, \quad (2)$$

$$n_+ \simeq m\omega_1 R_+^2 / \hbar, \quad (3)$$

$$n_- \simeq m\omega_1 R_-^2 / \hbar. \quad (4)$$

It is often convenient to consider the radial motion of an ion in a Penning trap in a frame which is rotating at $\Omega/2$ relative to the laboratory. In this frame the Lorentz force due to the magnetic field is exactly canceled by the Coriolis force arising from the rotation. The rotation also modifies the radial potential so that the ion behaves as if it were in a two-dimensional simple harmonic potential well

*d.segal@imperial.ac.uk

corresponding to the angular frequency ω_1 . The magnetron and modified cyclotron modes then correspond to clockwise and counterclockwise rotations around the magnetic field vector at ω_1 [14,15]. Since the motion in this frame is simple harmonic, equipartition of energy applies, and the average potential and kinetic energies are equal. In the laboratory frame, the modified cyclotron and magnetron motions form an epicyclic orbit in the plane perpendicular to the magnetic field. The electrostatic potential energy is negative, and the velocity corresponding to the cyclotron (magnetron) motion is increased (decreased) as a result of the transformation from the rotating frame to the laboratory frame. Therefore, equipartition of energy does not apply in the laboratory frame. Resolved-sideband spectroscopy only probes the kinetic energy of the modes.

The axial and cyclotron modes can be laser cooled by standard Doppler cooling. However, to reduce the amplitude of the magnetron motion, energy must be added to the mode. In the weak-binding regime this can be achieved by using a laser beam in the radial plane which has a gradient of intensity across the center of the trap. For more details see Refs. [12,16]. In this paper we show that, in the resolved-sideband regime, we can address sidebands due to both the magnetron mode and the cyclotron mode spectrally, as predicted in Ref. [13].

III. EXPERIMENTAL APPARATUS

We use a $^{40}\text{Ca}^+$ ion in this experiment. The internal energy-level diagram is shown in Fig. 1. Laser cooling utilizes the 397-nm $S_{1/2} \leftrightarrow P_{1/2}$ transition, which has a linewidth of 21 MHz. In our experiment all the transitions are split by the magnetic field used for confinement. The field strength is 1.85 T, corresponding to a cyclotron frequency of 705 kHz. Spontaneous decay on the $P_{1/2} \leftrightarrow D_{3/2}$ transition removes the ion from the cooling cycle, so the $D_{3/2}$ states need to be repumped. The magnetic field also mixes states with different values of J but the same values of L and M_J . This J -mixing process means that decay also occurs (very weakly) on the $P_{1/2} \leftrightarrow D_{5/2}$ transition, which is highly forbidden in the absence of a magnetic field [17]. Therefore, to maintain a closed system, the $D_{5/2}$ states also need to be

repumped. The branching ratio $\gamma(P_{1/2} \leftrightarrow D_{5/2})/\gamma(P_{1/2} \leftrightarrow S_{1/2})$ is approximately $4 \times 10^{-7} B^2$. Two lasers, one centered at 866 nm and one at 854 nm, are modulated using a single broadband electro-optic modulator to produce all ten laser frequencies that are necessary to repump these long-lived states.

At the end of the laser-cooling stage we expect the ion to be in a thermal state which can be decomposed into number states as $P(n) = \bar{n}^n / (\bar{n} + 1)^{n+1}$, where \bar{n} is the mean vibrational quantum number and \bar{n} can refer to \bar{n}_z , \bar{n}_+ , or \bar{n}_- . To perform motional spectroscopy the electric quadrupole allowed 729-nm $S_{1/2} \leftrightarrow D_{5/2}$ transition is probed. The oscillation frequencies are greater than both the spontaneous decay rate ($\sim 1 \text{ s}^{-1}$) [18] and the laser linewidth; therefore resolved sidebands rather than a continuous Doppler-broadened profile are observed. In the low-intensity limit and when the residual Doppler broadening is much greater than the vibrational frequency, we expect to observe many sidebands underneath an approximately Gaussian envelope [19]. From a quantum-mechanical point of view, the spectrum consists of a weighted average of spectra corresponding to each number state n . For $n = 0$ the spectrum is highly asymmetric as no transitions to a lower value of n are possible. For high n there is a negligible asymmetry in each spectrum, and the amplitude of each sideband is then given by a Bessel function whose argument depends on n . The sum of these spectra for a thermal state gives a final spectrum whose sideband amplitudes follow a Gaussian profile, as in the classical picture [19].

A description of the optical setup of our trap can be found in Ref. [20]. The trap consists of a stack of concentric cylindrical electrodes (see Fig. 2). Laser cooling beams at 397, 866, and 854 nm are directed towards the trap center, along the trap axis. A cooling beam at 397 nm is also applied in the radial plane. The offset of this beam is adjusted to alter the intensity gradient across the center of the trap to optimize the laser cooling. The 729-nm beam, which is derived from a laser diode, is stabilized using a Pound-Drever-Hall locking technique to an ultrahigh-finesse Fabry-Pérot cavity. It can be directed either along the trap axis or in the radial plane. Fluorescence light passes through two holes in the ring electrode, is focused onto optical fibers, and is detected by independent photomultipliers.

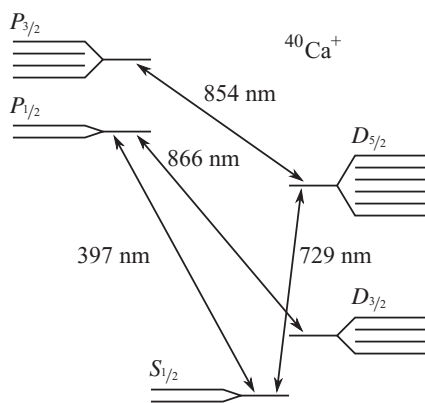


FIG. 1. Energy-level diagram of the levels addressed in our spectroscopy experiment (not to scale). The levels are split by the trapping magnetic field by tens of gigahertz.

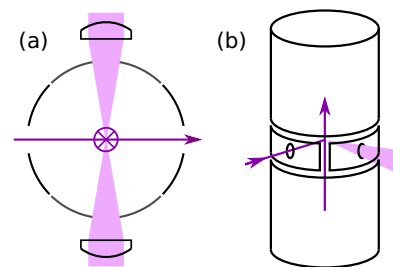


FIG. 2. (Color online) (a) Cross section of the trap through the split-ring electrode showing the apertures for laser access and fluorescence collection. The vertical laser beam is shown by a cross. (b) Schematic diagram of the trap with two hollow endcaps above and below the split-ring electrode. Laser beams are shown in purple (dark gray), and fluorescence is shown in light purple (light gray). The internal diameter of the trap is 21.6 mm, and the separation of the two endcap electrodes is 11.8 mm.

IV. RESULTS

The pulse sequence used to obtain spectra of the electric quadrupole transition is controlled by a field-programmable gate array with 20-ns timing resolution and is synchronized with the mains power supply to reduce stray ac magnetic fields. We first Doppler cool the ion for 5 ms using both 397-nm lasers. We then apply 729-nm radiation for 0.03–5.00 ms to drive the forbidden $S_{1/2} \leftrightarrow D_{5/2}$ transition. Just prior to this 729-nm pulse, the ion is optically pumped into the appropriate magnetic $S_{1/2}$ sublevel. The 729-nm pulse should place the ion in a superposition of the $S_{1/2}$ and $D_{5/2}$ states. We then perform a projective measurement of the state of the ion by reapplying the cooling lasers and counting photons emitted in a 5-ms interval. During the 729-nm pulse and the measurement we do not apply any 854-nm light, but it is otherwise kept on. The 866-nm laser is kept on throughout the experiment. This pulse sequence is typically repeated 100 times at each 729-nm laser frequency. We ensure that we do not oversaturate the $S_{1/2} \leftrightarrow D_{5/2}$ transition, so all the spectra we present here have a maximum shelving probability of <0.5 .

A. Axial spectrum

Figure 3 shows the probability of excitation as a function of the frequency of the 729-nm laser, with this laser directed along the magnetic-field direction. A clear sideband structure is seen having an overall width of approximately 1.5 MHz. The sidebands are spaced by $\omega_z/2\pi = 169$ kHz, the calculated value for a 40-V trap bias. The sidebands have a linewidth of approximately 20 kHz, which is determined primarily by the laser pulse duration.

We fit the data to a sideband spectrum corresponding to a thermal distribution. We include a dc offset to take into account the instances where the ion occasionally stops fluorescing during detection due to J -mixing, as described earlier. The

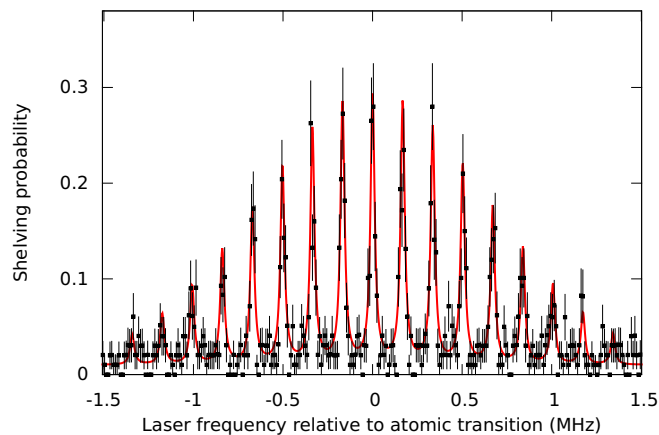


FIG. 3. (Color online) Spectrum of the axial motion of the ion recorded at a trap potential of 40 V, giving an axial oscillation frequency of 169 kHz; the laser frequency step was 10 kHz. The fit (solid line) is the product of equally spaced Lorentzian sidebands and a Gaussian envelope. This fit implies a temperature of $T = 1.1 \pm 0.2$ mK ($\bar{n} = 130 \pm 25$). The error bars reflect the statistical uncertainty in the shelving probability arising from the number of repetitions of the measurement cycle at each frequency step.

probability of this taking place during the counting period is approximately 2%, and it gives a constant background in the spectrum [17]. The fit suggests a temperature of 1.1 ± 0.2 mK or a mean occupation number of $\bar{n} = 130 \pm 25$. This should be compared to the Doppler cooling limit for this mode of 0.38 mK or an occupation number of $\bar{n}_z = 47$. There are several possible reasons why the measured value is greater than the calculated Doppler limit. These include the effects of saturation of the laser cooling transition and uncertainty in the detuning of the cooling lasers. There is also an effect due to the steady-state displacement of the ion in the cooling beams. When these beams are turned off abruptly, the motion of the ion is excited [11]. We estimate that in our case the axial displacement of $\sim 0.3 \mu\text{m}$ gives the ion an additional energy equivalent to a temperature increase of approximately 0.25 mK.

B. Radial spectrum

Figure 4 shows data recorded when the 729-nm beam is incident on the ion in the radial plane. The spectrum shows cyclotron sidebands with a spacing of approximately 700 kHz, with each cyclotron sideband having a set of magnetron sidebands which are unresolved at this trap bias. The relative width of the comb of magnetron sidebands compared to the overall span of the cyclotron sidebands clearly demonstrates that the velocity distribution for the magnetron motion is much narrower than that of the modified cyclotron motion. In order to reduce the time needed to record this spectrum data were only taken around the frequencies where sidebands are expected to occur.

We perform a Gaussian fit to the amplitudes of the cyclotron sidebands, giving a FWHM of 4 ± 1 MHz, which corresponds to a temperature of 7 ± 3 mK and $\bar{n}_+ \sim 200$. This observed temperature depends sensitively on the laser parameters. Our calculations based on Ref. [12] suggest that it should be possible to achieve a temperature of ~ 0.8 mK. However, this

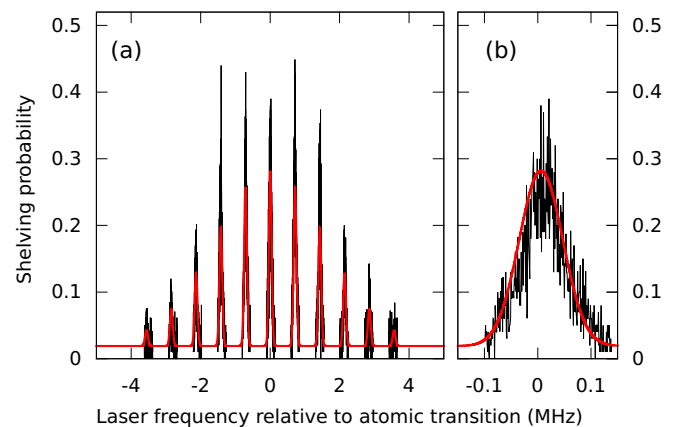


FIG. 4. (Color online) (a) Radial spectrum showing modified cyclotron sidebands, each of which is broadened due to the magnetron motion. Magnetron sidebands cannot be resolved fully at this trap voltage (5 V) because they are spaced by only 2.5 kHz. (b) Expanded detail of the carrier transition, showing the partially resolved magnetron sidebands. A fit to a Gaussian profile can be used to gain a rough idea of the width of the spectrum.

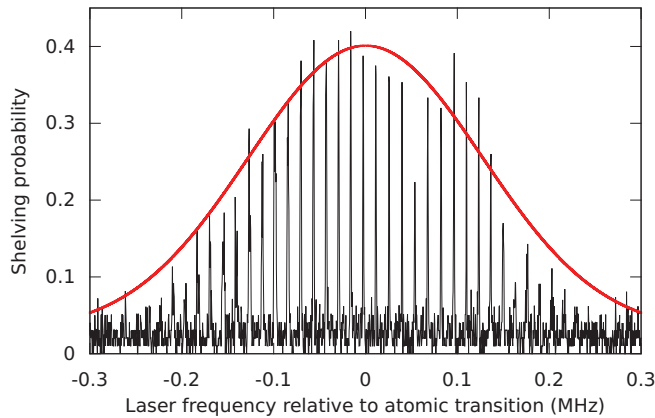


FIG. 5. (Color online) Spectrum of a single cyclotron sideband with resolved equally spaced 15-kHz magnetron sidebands. The large variation of the heights of the sidebands is due to the fact that there is typically only one data point close to the maximum. Each point on this graph was calculated from 100 repetitions of the pulse sequence.

is a function of the width, saturation, and detuning of the radial laser beams, which are not well known.

It is clear that the temperature derived from the Doppler width of the magnetron motion (approximately $4 \mu\text{K}$) is much less than the standard Doppler limit of $\sim 0.5 \text{ mK}$ for a calcium ion in a harmonic trap. This counterintuitive result arises because the magnetron mode is not cooled by velocity selection (as in standard Doppler cooling) but is rather due to the intensity gradient of the laser beam, as discussed above.

For the magnetron motion recorded in a separate experiment at a higher trap voltage (30 V) we once again observe a number of cyclotron sidebands, but this time they are convolved with a set of well-resolved magnetron sidebands with a spacing of 15 kHz (see Fig. 5). Individual sidebands are less than

1 kHz wide, giving an upper limit on the laser linewidth over a few seconds. By fitting a Gaussian profile to the peaks of a set of magnetron sidebands, as seen in Fig. 5, we find a FWHM of $301 \pm 21 \text{ kHz}$, corresponding to a temperature of $42 \pm 8 \mu\text{K}$ and $\bar{n}_- \sim 3000$. Again, this value is sensitive to changes in the laser parameters. In this case the minimum expected temperature is estimated to be $10 \mu\text{K}$.

V. CONCLUSION

In conclusion, we have measured optical sideband spectra for a single ion in a Penning trap. We have directly measured the kinetic temperature of all three modes of motion of the ion. In future work we expect to be able to laser cool the ion to the ground state using resolved-sideband cooling; we will then investigate the heating rates in the trap, which previously have only been measured using less sensitive techniques [21].

Resolved-sideband cooling of the axial motion will be implemented in the same way as is conventional in rf traps. Our scheme for sideband cooling of the radial motion is more complicated because the magnetron mode is initially in a relatively high quantum state and has a negative total energy. We initially intend to apply resolved-sideband cooling to an individual ion in a Penning trap and then also to small Coulomb crystals [20].

ACKNOWLEDGMENTS

This work was supported by the UK Engineering and Physical Sciences Research Council (Grant No. EP/D068509/1) and by the European Commission STREP PICC (FP7 2007-2013 Grant No. 249958). We gratefully acknowledge financial support towards networking activities from COST Action MP 1001-Ion Traps for Tomorrow's Applications.

-
- [1] J. C. Bergquist, W. M. Itano, and D. J. Wineland, *Phys. Rev. A* **36**, 428 (1987).
 - [2] H. S. Lakkaraju and H. A. Schuessler, *J. Appl. Phys.* **53**, 3967 (1982).
 - [3] A. Schliesser, R. Rivière, G. Anetsberger, O. Arcizet, and T. J. Kippenberg, *Nat. Phys.* **4**, 415 (2008).
 - [4] S. E. Hamann, D. L. Haycock, G. Klose, P. H. Pax, I. H. Deutsch, and P. S. Jessen, *Phys. Rev. Lett.* **80**, 4149 (1998).
 - [5] A. M. Kaufman, B. J. Lester, and C. A. Regal, *Phys. Rev. X* **2**, 041014 (2012).
 - [6] J. D. Thompson, T. G. Tiecke, A. S. Zibrov, V. Vuletic, and M. D. Lukin, *Phys. Rev. Lett.* **110**, 133001 (2013).
 - [7] F. Diedrich, J. C. Bergquist, W. M. Itano, and D. J. Wineland, *Phys. Rev. Lett.* **62**, 403 (1989).
 - [8] B. P. Lanyon, C. Hempel, D. Nigg, M. Müller, R. Gerritsma, F. Zähringer, P. Schindler, J. T. Barreiro, M. Rambach, G. Kirchmair, M. Hennrich, P. Zoller, R. Blatt, and C. F. Roos, *Science* **334**, 57 (2011).
 - [9] L. S. Brown and G. Gabrielse, *Rev. Mod. Phys.* **58**, 233 (1986).
 - [10] T. Monz, P. Schindler, J. T. Barreiro, M. Chwalla, D. Nigg, W. A. Coish, M. Harlander, W. Hänsel, M. Hennrich, and R. Blatt, *Phys. Rev. Lett.* **106**, 130506 (2011).
 - [11] B. C. Sawyer, J. W. Britton, A. C. Keith, C.-C. J. Wang, J. K. Freericks, H. Uys, M. J. Biercuk, and J. J. Bollinger, *Phys. Rev. Lett.* **108**, 213003 (2012).
 - [12] W. M. Itano and D. J. Wineland, *Phys. Rev. A* **25**, 35 (1982).
 - [13] D. J. Wineland, W. M. Itano, J. C. Bergquist, and R. G. Hulet, *Phys. Rev. A* **36**, 2220 (1987).
 - [14] R. C. Thompson and D. C. Wilson, *Z. Phys. D* **42**, 271 (1997).
 - [15] M. Asprusten, S. Worthington, and R. C. Thompson, *Appl. Phys. B* **114**, 157 (2014).
 - [16] R. C. Thompson and J. Papadimitriou, *J. Phys. B* **33**, 3393 (2000).
 - [17] D. R. Crick, S. Donnellan, D. M. Segal, and R. C. Thompson, *Phys. Rev. A* **81**, 052503 (2010).
 - [18] P. A. Barton, C. J. S. Donald, D. M. Lucas, D. A. Stevens, A. M. Steane, and D. N. Stacey, *Phys. Rev. A* **62**, 032503 (2000).
 - [19] D. J. Wineland and W. M. Itano, *Phys. Rev. A* **20**, 1521 (1979).
 - [20] S. Mavadia, J. F. Goodwin, G. Stutter, S. Bharadia, D. R. Crick, D. Segal, and R. C. Thompson, *Nat. Commun.* **4**, 2571 (2013).
 - [21] M. J. Jensen, T. Hasegawa, and J. J. Bollinger, *Phys. Rev. A* **70**, 033401 (2004).